Preparation of magnesium and zinc aluminate spinels by microwave heating: Influence of the oxide precursors on the phase composition

Justin Chassagne, Clémence Petit, Christophe Meunier, François Valdivieso

Preparation of magnesium and zinc aluminate spinels by microwave heating: Influence of the oxide precursors on the phase composition

Justin CHASSAGNE, Clémence PETIT*, Christophe MEUNIER, François VALDIVIESO

Mines Saint-Étienne, Université de Lyon, CNRS, UMR 5307 LGF, Centre SMS, F-42023 Saint-Étienne France

*Corresponding author: Clémence PETIT, clemence.petit@emse.fr

Mines Saint-Etienne, Université Lyon, CNRS, UMR 5307 LGF, Centre SMS, F-42023 Saint-Etienne, France, Phone : +33 4 77 42 02 23

Abstract

This study focuses on understanding the difference between conventional and microwave (MW) heating to obtain magnesium and zinc aluminate spinels ($MgAl_2O_4$ and $ZnAl_2O_4$) starting from raw oxide powders (magnesia/alpha-alumina, magnesia/gamma-alumina and zincite/alpha-alumina mixtures). The samples were prepared from these different oxide precursors and submitted to different thermal cycles in a MW multimode cavity. The evolution of phase composition was studied by X-Ray Diffraction (XRD) analysis. The choice of the precursors aimed at studying the influence of the difference of dielectric properties and of the specific surface area on the phase formation under MW. It was shown that spinel phases could be obtained by rapid MW thermal cycles (*i.e.*, 100 °C/min under MW vs 25 °C/min under conventional heating). The presence of ZnO as a MW absorbent was beneficial for the MW/material interactions. But, for the three considered mixtures, a SiC susceptor was necessary to facilitate heating.

Keywords: Spinel, microwave, dielectric properties

1. Introduction

In recent decades, microwave (MW) heating has increasingly been used in response to various issues in the field of ceramics[1]. Indeed, this technology is known to be faster and greener than conventional heating with an electric furnace, and some studies have shown evidence that it could improve material microstructures and properties[2–4]. Moreover, this technology is able to perform both the synthesis of oxide powders[5] and the sintering of materials[6]. These advantages are derived from the heating process: the ceramics are directly heated by interaction with the MW field. This leads to fast volumetric heating. Consequently, the temperature inside the sample is more homogeneous than it is with conventional heating. However, MW sintering is highly dependent on the dielectric properties of the material, especially the dielectric loss tangent ($\tan \delta = \varepsilon''/\varepsilon'$, with ε' and ε'' being the real and the imaginary part of the permittivity, respectively)[7]. When ceramics have a high dielectric loss, they can be heated by a direct interaction with the MW. Conversely, when materials have a low dielectric loss or are transparent to MW, a susceptor must be added around the sample to obtain hybrid or indirect heating, respectively. This susceptor is made of a material with high dielectric loss in order to couple with microwaves and heat the sample by infrared radiation. Silicon carbide (SiC) is generally used[8, 9].

Magnesium aluminate ($MgAl_2O_4$) and zinc aluminate ($ZnAl_2O_4$) spinels have been widely studied because they exhibit a high melting point, high mechanical strength and hardness, especially at high temperatures[10, 11]. When they are fully dense, they exhibit high transparency in the visible and IR-wavelength ranges[12,13], making them useful for a wide range of applications: armored windows, protective window lasers, or jewelry[11]. $MgAl_2O_4$ and $ZnAl_2O_4$ can be obtained from raw spinel powders *via* different sintering processes: conventional pressureless sintering, hot isostatic pressing or spark plasma sintering[12,14–17]. A second approach consists in reactive sintering, where spinel is generally obtained from a mixture of oxide

precursors, *i.e.*, α-alumina (α-Al_2O_3) and magnesia (MgO) mixture[18, 19] or α-alumina (α-Al_2O_3) and zincite (ZnO) mixture[20]. MW sintering has been applied to spinel material to sinter spinel powder[15, 21–23]. Few authors have studied the MW sintering of spinel from a mixture of oxides[24] or the MW synthesis of spinel powder from different precursors[25–28], and these authors did not systematically deepen the investigation about the understanding of MW/materials interaction in relation with the choice of the precursors.

The main aim of this paper is to study a possible positive effect of MW heating on the formation of $MgAl_2O_4$ and $ZnAl_2O_4$ spinel phases from three different precursor systems: MgO/α-Al_2O_3, MgO/γ-Al_2O_3 and ZnO/α-Al_2O_3. These three systems were used to study the influence of two parameters on the MW/material interactions: the difference of electrical and dielectric properties of the oxide precursors and the specific surface area of the raw powders. MgO/α-Al_2O_3 and ZnO/α-Al_2O_3 mixtures differ by their dielectric and electrical properties. MgO/α-Al_2O_3 is a mixture of two low coupling materials (electrical insulator[27,29]), whereas ZnO/α-Al_2O_3 is a mixture of a MW absorbent (ZnO is a semi-conductor[30]) and a low MW absorbent (α-Al_2O_3 is an electrical insulator). Therefore, we can hypothesize that the ZnO/α-Al_2O_3 mixture can couple better with MW than the MgO/α-Al_2O_3 one. Because of the similar coupling ability with MW of MgO and α-Al_2O_3, this mixture was used to test the influence of the specific surface area of the raw powder. The higher specific surface area of γ-Al_2O_3 (compared to α-Al_2O_3) can favour a higher reactivity between the alumina powder the other powder in the mixture. For this purpose, γ-Al_2O_3 powder (which is a transitional alumina having a higher specific surface area than α-Al_2O_3 powder, see Figure 1) was also mixed with MgO.

The mixtures were heated with different thermal cycles in a MW multimode cavity. The spinel formation was investigated by X-Ray Diffraction (XRD) analysis. The conditions of the MW thermal treatments (especially, the influence of a susceptor) was also studied.

2. Materials and methods

2.1. Sample preparation

Four different commercial pure ceramic oxide powders were used in this study: α-Al_2O_3 BA15 from Baikowski (d_{50} = 10 µm; S_{BET} = 15 m²/g), γ-Al_2O_3 CR125 from Baikowski (d_{50} = 0.3 µm; S_{BET} = 105 m²/g), MgO from Prolabo (d_{50} = 7.6 µm) and ZnO from Fluka (d_{50} = 2.3 µm). Three equimolar mixtures were made from these powders: α-Al_2O_3/MgO, γ-Al_2O_3/MgO and α-Al_2O_3/ZnO. In order to get a good homogenization, an organic binder was added. To do so, the total amount of powder was put in a mixture of 1.5 wt% of polyethylene glycol (PEG 1500, Merck) and 1 wt% of polyvinylbutyral (PVB, Sigma-Aldrich) in ethanol, until it reaches 60 w% of ceramic in the suspension. Afterwards, the suspension was dried in a furnace set at 60 °C during few hours. Once the ethanol was evaporated, the agglomerates were milled by ball milling with alumina balls (Φ = 2 mm and 10 mm) and then sieved to get agglomerate size under 200 µm. For the different experiments, the blends of ceramic powders were shaped into compact cylindrical pellets by uniaxial compression until a pressure of 300 MPa (Model 5584, INSTRON, USA). As heating devices are different depending on whether a CV furnace or a MW cavity is used, the dimensions of the pellets are different: a diameter of 8 mm and a height of around 7 mm is needed for conventional (CV) heating experiments and a diameter of 12 mm with a height of about 5 mm is needed for MW experiments. These pellets were then debinded at 600 °C during 30 minutes under air atmosphere with a heating rate of 1 °C/min.

2.2. MW setup

To initiate spinel formation with MW, an instrumented multimode MW set-up shown in Figure 2 was used. It has previously been described by Zymelka *et al.*[31] and Zuo *et al.*[32]. MW heating takes place in a multimode cavity where MW are conducted through a rectangular waveguide. The source (GMP30K, SAIREM, France) works at 2.45 GHz and is able to deliver power up to

2 kW. A mixing paddle allows a homogeneous electromagnetic field into the MW cavity. The sample is placed in the middle of the cavity, into an insulation box made of thermal insulators and the susceptor (see Figure 2a). This insulation box has been developed during previous work[32]. The thermal insulators are plates of aluminosilicate fibers (KVS 184–400, Rath®, Germany). Rath® fulfils the requirements for MW applications: it is a refractory material transparent to MW, is resistant to temperatures up to 1800 °C and has a low thermal conductivity (0.33 $W.m^{-1}.K^{-1}$ at 1400 °C) to maintain good thermal homogeneity during heating. The pellet is placed with its circular surface down (to allow temperature measurement on its flat face) on two alumina rods (see Figure 2a). The pellet and the two rods are placed inside a mullite tube. A SiC ring, used as a susceptor, surrounds the mullite tube. This material is chosen for its high dielectric loss at low temperatures, which allows the initiation of the heating process at ambient temperature. The mullite tube protects the sample from the high radiation of the susceptor and ensures more homogeneous heating of the sample. As conventional thermocouples cannot be employed because they interact with MW and affect the electromagnetic field distribution inside the cavity, temperature was measured by pyrometry. A bichromatic infrared pyrometer (Lumasense Technology, Germany) placed at around 40 cm from the sample was used (Figure 2b shows the position of the pyrometer with respect to the sample). This pyrometer was sensitive to the wavelengths between 2 and 2.5 μm and worked in the 250-1800 °C temperature range. The emissivity ratio was set to 1. The front of the insulation box contained a hole to enable the temperature measurement of the sample on its flat surface.

Before starting the temperature recording and to initiate the heating, the incident power was set at 500 W until reaching 250 °C. Next, the heating cycle was controlled with home-made LabVIEW software. A PID controller was used to adjust the incident power delivered by the generator, in relation to the temperature measured by the pyrometer, to match the measured

temperature with the set temperature. An impedance tuner was also manually adjusted to minimize the reflected power. Other data were also recorded during the heating cycle (temperature and absorbed, reflected and incident powers).

2.3. Heating cycles

Different sets of experiments were applied to the pellets.

First of all, the influence of the insulation box (and especially the susceptor) was studied. For this purpose, a first heating cycle was applied to ZnO/α-Al_2O_3 pellets with two different configurations of the insulation box (*i.e.*, with and without the SiC ring). These experiments were carried out with the ZnO/α-Al_2O_3 mixture because it is considered as the easiest to heat under MW, so the easiest to heat without susceptor (due to the favourable dielectric properties of ZnO). The pellets were submitted to the following heating cycles: temperature of 1150 °C, heating rate of 50 °C/min without holding time. This heating cycle was applied with and without the SiC ring in the insulation box. The temperature was chosen according to preliminary works showing that at this temperature, 50 %mol spinel was obtained in the pellet (not shown here).

Then, a constant MW incident power of 1200 W was sent to the cavity and the temperature reached by the pellet was measured by the pyrometer. The temperature vs time curve was then used to calculate the instantaneous heating rate of the pellets. This experiment was also carried out for ZnO/α-Al_2O_3 pellet with and without the SiC ring. The heating experiments with and without the susceptor aimed at understanding better the coupling capability.

Next, the best configuration of the insulation box was chosen to apply different heating cycles to the three types of pellets. The following types of heating cycles were tested: varying temperatures (from 800 to 1500 °C with fixed heating rate and dwell time), varying heating rates (10, 25 and 50 °C/min with fixed temperature and dwell time), and varying dwell times (0, 15, 30 and 60 minutes with fixed temperature and dwell time). The temperatures were

chosen according to the results of preliminary X-ray diffraction analyses carried out on pellets conventionally heated at different temperatures (results not shown here).

For comparison purposes, some pellets were conventionally heated in a dilatometer (Setsys 16/18; SETARAM, Caluire, France, equipped with the software Calisto) where the temperature was measured with thermocouples. The following thermal cycle was applied: heating rate of 25 °C/min until the desired temperature (depending on the mixture), and no dwell time.

The results of these different heating cycles will be presented in the different subsections of the section 3.

2.4. XRD characterization

After the different heating treatments, the pellets were manually ground into powder and X-ray analyses were carried out in order to determine the different phase contents. XRD analysis was performed on a diffractometer (D8A25, Bruker, Germany, equipped with LynxEye XE T detector) with a Cu Kα radiation (wavelength = 1.5406 Å) with the following parameters: angular range $20 < 2\theta < 80$; angular step of 0.02; rotation of 10 rpm; acquisition time of 550 sec; and an entry slot fixed at 0.3. A motorized knife was used for the suppression of the scattered background at low angles without altering the data at high angles. Data processing was performed with the software Diffrac.EVA and the database PDF4+. The XRD diffractograms were then compared with the files from the International Centre for Diffraction Data (ICDD) generated by the PDF-4+ software: n° 00-010-0425 (γ-Al_2O_3); n° 00-046-1212 (α-Al_2O_3); n° 00-043-1022 (MgO); n° 00-036-1451 (ZnO); n° 00-021-1152 ($MgAl_2O_4$) and n° 00-005-0669 ($ZnAl_2O_4$). The quantification of each phase with an accuracy of ± 1 % was then carried out with the Rietveld refinement method using the TOPAS software. This software uses ICDD diffractograms of each compound theoretically present in the powder analyzed and adjusts their parameters to fit them as far as possible with the experimental diffractogram. To

determine its exact composition by weight, the whole diffractogram was taken into account. Then the mass percentage was turned into a molar composition.

3. Results and discussion

3.1. Study of the impact of the susceptor on MW heating

The mixtures were made of different materials that do not have the same dielectric properties. Therefore, the interaction of the mixtures with MW was studied first. To do so, a comparison between hybrid heating (with SiC susceptor) and direct heating (without SiC susceptor) was made on ZnO/α-Al_2O_3 mixtures. These samples were heated to 1150 °C, with a heating rate of 50 °C/min. The diffractograms of the ground heated pellets are shown in Figure 3. The $ZnAl_2O_4$ phase is detected in the two samples. The initial phases (ZnO and α-Al_2O_3) are also present, especially in the sample heated without SiC. Table 1 presents the spinel content formed (%mol) in the two powder mixtures. It is observed that the time needed to initiate the sample heating (temperature > 250 °C) is significantly higher without the susceptor (∼ 30 min) than with the susceptor (∼ 3 min). In the diffractograms, the peaks corresponding to $ZnAl_2O_4$ have a higher intensity for hybrid heating than for direct heating. It is confirmed by the quantification: a higher spinel content is reached when a SiC susceptor is used. Therefore, direct heating is less efficient and slower than hybrid heating and the same results are obtained whatever the oxides used. That means that even if ZnO couples with MW, the low dielectric loss of Al_2O_3 reduces the coupling of the mixtures.

Figure 4 shows the temperature measured at the surface of the ZnO/α-Al_2O_3 sample, with and without SiC susceptor, with a heating rate set at 50 °C/min. At the beginning, the heating rate cannot be reached without a susceptor, even with the MW source at maximum power. After 500 °C, the temperature rate increases until the set temperature is reached. Without a susceptor, ZnO does not couple enough with MW at low temperatures to follow the set temperature ramp.

Therefore, a SiC susceptor is necessary to heat samples with high heating rates and to allow good control of the temperature ramp.

The evolution of the instantaneous heating rate vs temperature for the pellets submitted to a constant MW incident power of 1200 W was studied for ZnO/α-Al_2O_3 with and without SiC. The results are presented in Figure 5a. In the case of heating with the SiC susceptor, the heating rate is quite stable (around 30-50 °C/min), which means that the MW absorption is constant. However, when the SiC ring is not used, the sample is heated slowly at a low temperature but a high heating rate is reached after 800 °C (more than 50 °C/min and up to 100 °C/min). The observation of a mullite tube's radiation indicates that it couples with MW after 800 °C, and this phenomenon likely leads to the rise of the sample heating rate. As a consequence, the mullite tube seems to act as a susceptor at high temperatures. To check this point, the same experiment was applied to another pellet (*i.e.*, MgO/γ-Al_2O_3) for which the dielectric properties are different (see Figure 5b).

By comparing the evolution of the heating rate of the ZnO/α-Al_2O_3 and MgO/γ-Al_2O_3 samples without susceptor (Figure 5b), a difference in MW absorption is observed. The MgO/γ-Al_2O_3 mixture's heating rate gradually increases until it reaches a maximum rate of 90 °C/min near 1100 °C, whereas a quick increase in the heating rate of the ZnO/α-Al_2O_3 mixture is first observed after 800 °C, with a maximum near 875 °C, before another rise to 1050 °C. The progressive increase in the heating rate to 1100 °C may correspond to the radiation of the mullite tube. However, the quick heating rate rise to 800 °C in the ZnO/α-Al_2O_3 shows that ZnO couples with MW sufficiently at high temperatures to initiate the heating of the sample. It is shown that the ZnO/α-Al_2O_3 does not couple sufficiently to initiate spinel formation, but the results in Figure 4b prove that the difference in dielectric properties between the two mixtures (*i.e.,* ZnO/α-Al_2O_3 and MgO/γ-Al_2O_3) can be visible from 800 °C. This observation means that even if ZnO does not absorb enough MW at ambient temperature to

initiate the heating, it does at higher temperature and hybrid heating occurs. Indeed, the ZnO semi-conductor presents high losses (ε") and a higher conductivity at high temperatures, which leads to a rise in the heating rate.

This study shows that the spinel phase has been detected after direct or hybrid MW heating. However, the use of a SiC ring as a susceptor is necessary to take full advantage of MW heating (*i.e.*, high heating rates, quick heating, high spinel formation). It has also been shown that even if ZnO absorbs MW at high temperatures, this is not enough to initiate the heating of the mixture at ambient temperature. Therefore, a SiC susceptor is needed whatever the mixture heated.

3.2. Spinel formation under hybrid MW heating

The impact of the MW heating rate was studied by analyzing the composition of the ground pellets heated at 1400 °C. Three ramps were selected: 10 °C/min, 25 °C/min and 50 °C/min. The diffractograms of the heated ground pellets are presented in Figure 6. The spinel content (%mol) in each mixture is reported in Table 2. The diffractograms of the MgO/α-Al_2O_3 and MgO/γ-Al_2O_3 mixtures exhibit the peaks corresponding to MgO, α-Al_2O_3 and $MgAl_2O_4$ phases. It is in accordance with the spinel molar contents obtained for these mixtures. For ZnO/α-Al_2O_3 (Figure 6c), the peaks matching the $ZnAl_2O_4$ phase are the most intense ones (in relation with the high spinel content reached in these samples). It is related to the high spinel content reached at 1400 °C. The conversion rate of the powder mixture into a spinel powder at 1400 °C depends on numerous parameters. First, the higher the temperature ramp, the lower the conversion rate. Indeed, spinel formation is a function of time and a high heating rate obviously leads to a low conversion. However, the difference between a heating rate of 25 °C/min and one of 50 °C/min is not significant. Concerning the ZnO/α-Al_2O_3 mixture, a high spinel content is already reached at 1400 °C. Thus, it is not possible to draw any conclusion about the impact of the heating rate on this mixture.

Finally, the spinel content at 1400 °C depends on the initial powder composition and the heating rate. A heating rate of 50 °C/min was chosen for the following experiments.

3.2.1. Spinel content evolution with temperature

The temperature-dependent spinel formation was followed by XRD analyses (diffractograms not shown here) on these three different samples, shown in Figure 7. According to these results, it is possible to determine the point at which spinel starts to form. From the MgO/α-Al_2O_3 mixture, $MgAl_2O_4$ appears after 1000 °C. In the same way, $ZnAl_2O_4$ spinel appears after 900 °C. Unlike the mixture with α-Al_2O_3, the $MgAl_2O_4$ spinel formed from γ-Al_2O_3 appears before 800 °C. This is due to a better reactivity of γ-Al_2O_3 with MgO. These results are in agreement with observations found in the literature for CV heating[33–35]. Therefore, MW heating does not affect the temperature at which the reaction starts.

However, reaction kinetics depend on the initial powder composition. Thus, the formation of $ZnAl_2O_4$ spinel from ZnO and α-Al_2O_3 is faster than the $MgAl_2O_4$ spinel formation from MgO and α-Al_2O_3. Moreover, while MgO starts to react quickly with α-Al_2O_3 at 1000 °C, its reaction with γ-Al_2O_3 starts much sooner and more slowly. Therefore, spinel concentration in the powder is higher for the MgO/α-Al_2O_3 sample after 1200 °C while it is higher for the MgO/γ-Al_2O_3 sample before 1200 °C.

3.2.2. Spinel content evolution with time

The spinel formation kinetics at a given temperature were studied with different dwell times: 0, 15, 30 and 60 minutes. The temperature chosen was the one which occurred when 50 %mol of spinel was formed in the mixtures: 1350 °C for MgO/α-Al_2O_3, 1450 °C for MgO/γ-Al_2O_3 and 1150 °C for ZnO/α-Al_2O_3. Pellets were heated at 50 °C/min until they reached these temperatures. The sample composition was then determined by XRD analyses

(diffractograms not shown here) and the spinel content was quantified with the Rietveld refinement method. The kinetic curves obtained are shown in Figure 8a. The reaction rate constant *k* (related to the kinetic of the reaction) was determined with a linear regression, as the powders were added to the mixture in stoichiometric molar proportions. Thus, all the reaction kinetics can be expressed by equation 1:

$$[Al_2O_3] + [MgO] = [MgAl_2O_4] \qquad eq.1$$

The reaction rate of spinel formation is equal to the reaction rate of alumina consumption and can be defined by equation 2:

$$v = \frac{d[MgAl_2O_4]}{dt} = -\frac{d[Al_2O_3]}{dt} = k.[Al_2O_3].[MgO] = k.[Al_2O_3]^2 \qquad eq.2$$

Integration of equation 2 gives the evolution of Al_2O_3 content depending on time (equation 3):

$$\frac{1}{[Al_2O_3]} = k \times t + \frac{1}{[Al_2O_3]_0} \qquad eq.3$$

Where $[Al_2O_3]$ is the current Al_2O_3 content,

$[Al_2O_3]_0$ is the initial Al_2O_3 content

The reaction rate constant *k* ($\%mol^{-1}.s^{-1}$) can be determined from the slope of the linear regression of $1/[Al_2O_3] = f(t)$. The results are presented in Figure 8b and show that, as expected, the reaction between the oxides to form the spinel phase has an order 2 kinetic. The $ZnAl_2O_4$ has a higher formation rate than the $MgAl_2O_4$ obtained from α-Al_2O_3. Moreover, the type of alumina used has an impact on the spinel formation kinetic. Indeed, after 1300 °C almost all the γ-Al_2O_3 is transformed into α-Al_2O_3. However, the γ-Al_2O_3 used seems to lead to a highest spinel formation rate. That is probably due to the highest specific surface area of the γ-Al_2O_3 particles, which allow a larger contact surface with the MgO powder than between α-Al_2O_3 and MgO powders.

The reaction rate constant *k* also depends on the temperature, as demonstrated by the Arrhenius equation 4:

$$k(T) = Ae^{-\frac{Ea}{RT}} \qquad eq.4$$

Therefore, depending on the temperature reached for the kinetic measurement, the reaction rate constant differs. To see to what extent temperature affects the reaction rate, two kinetics were compared at 1350 and 1400 °C in the MgO/α-Al_2O_3 mixture (Figure 9). The slope of the linear regression of 1/[Al_2O_3] = f(t) leads to the reaction rate constants k_{1350} at 1350 °C and k_{1400} at 1400 °C. The reaction rate constant doubles when the temperature of the experiment is raised from 1350 to 1400 °C.

Therefore, it is difficult to compare each spinel formation rate because of the difference in spinel formation temperature, even though all measurements start when 50 %mol of spinel is formed.

3.3. Comparison of MW and CV heating

The study described above shows that it is possible to form spinels under MW heating from different oxide precursors (MgO/α-Al_2O_3, ZnO/α-Al_2O_3 or MgO/γ-Al_2O_3). Hybrid MW heating was preferred to direct MW heating because of its higher heating rate and efficiency. However, it is worth comparing these results with CV heating to determine whether a higher heating rate is the only advantage of MW heating, or whether there are other differences. Thus, a comparison between these two heating processes was performed. As a dilatometer furnace cannot reach high temperature ramps, a heating rate of 25 °C/min was chosen for this part of the study. The spinel content in the samples after heating to 1400 °C was measured by XRD analyses. The results in Table 3 show that a lower quantity of spinel $MgAl_2O_4$ is formed by MW heating than by CV heating (difference of approximately 40 %). At 1400 °C, the amount

of $ZnAl_2O_4$ formed is high, so the difference between the two kinds of heating process cannot be determined for ZnO/α-Al_2O_3.

The quantity of $MgAl_2O_4$ depending on the temperature was measured in a MgO/γ-Al_2O_3 sample heated at 25 °C/min by CV and MW heating treatments. The results are presented in Figure 10a. The two curves show a similar evolution but with an apparent temperature offset from the temperature of 1300 °C. When a shift of 100 °C to lower temperatures is applied to the MW results, the two curves overlap (Figure 10b). This difference can be due to different phenomena. Firstly, an inaccuracy in the temperature measurement method is probable. Indeed, during MW heating, the temperature is measured on the surface of the sample with a bichromatic pyrometer. The hypothesis of an emissivity ratio k=1 can be incorrect, and the right value has to be determined by a new calibration of the pyrometer. As demonstrated by Croquesel *et al.*[8], an error of 1% on the value of the emissivity ratio can lead to an uncertainty of 50 °C on the temperature measurement at high temperatures. Moreover, the evolution of dielectric and electrical properties of materials with temperature can also have an influence. It is especially the case for SiC. As temperature increases, the electrical conductivity of SiC increases[36]. It can lead to a less efficiency of SiC as susceptor because a major part of the MW can be absorbed volumetrically within the sample. Consequently, the temperature of the bulk of the sample can be higher than the one at the surface, which is measured by the pyrometer.

4. Conclusion

This work shows that MW heating of oxide precursor mixtures enables the formation of magnesium and zinc aluminate spinel phases with a yield of more than 90%. The presence of a SiC ring as a susceptor is preferred in order to obtain better results (*i.e.*, faster heating start, higher heating rates, and so greater efficiency). A higher heating rate was observed between

800 °C and 950 °C when the ZnO/α-Al_2O_3 mixture was used instead of the MgO/γ-Al_2O_3 mixture, with a constant MW power and without a SiC susceptor. Nevertheless, it did not have any impact on either the MW heating or the spinel formation. The type of alumina powder affected the temperature from which the spinel formation started, but both of them allowed the reaction to take place. The spinel formation kinetics demonstrated that the use of γ-Al_2O_3 (very high specific surface area) instead of α-Al_2O_3 led to higher formation rates. Moreover, the use of a ZnO precursor also led to higher spinel formation rates than using a MgO precursor. It might have been worth comparing spinel formation kinetics under MW and CV heating, but the difference in temperature measurement methods in this work would have provided incorrect results (a change of 50 °C showed a significant reaction rate constant difference). Finally, the comparison between MW and CV heating gave similar results in terms of spinel formation. However, MW heating enables higher heating rates and is greener. The next step will be to optimize the choice of thermal treatments to obtain fully dense spinel samples and then to characterize their properties. To go further in the comprehension of the reactivity under MW, it could be interesting to compare MW heating of pellets and powder beds.

Acknowledgements

The authors would like to thank Olivier Valfort at Mines Saint-Étienne for its assistance for XRD analyses.

This work was financially supported by ARMINES (no grant number).

References

1. Bykov YV, Rybakov KI, Semenov VE. High-temperature microwave processing of materials. *J Phys Appl Phys*. 2001;34(13):R55–R75. https://doi.org/10.1088/0022-3727/34/13/201
2. Xie Z, Yang J, Huang Y. Densification and grain growth of alumina by microwave processing. *Mater Lett*. 1998;37(4–5):215–220. https://doi.org/10.1016/S0167-577X(98)00094-9
3. Brosnan KH, Messing GL, Agrawal DK. Microwave sintering of alumina at 2.45 GHz. *J Am Ceram Soc*. 2003;86(8):1307–1312. https://doi.org/10.1111/j.1151-2916.2003.tb03467.x
4. Janney MA, Kimrey HD, Allen WR, Kiggans JO, Enhanced diffusion in sapphire during microwave heating. *J Mater Sci*. 1997;32(5):1347–1355. https://doi.org/10.1023/A:1018568909719
5. Prado-Gonjal J, Schmidt R, Morán E. Microwave-assisted routes for the synthesis of complex functional oxides. *Inorganics*. 2015;3(2):101–117. https://doi.org/10.3390/inorganics3020101
6. Zhu J, Ouyang C, Xiao S, Gao Y. Microwave sintering versus conventional sintering of NiCuZn ferrites. Part I: Densification evolution. *J Magn Magn Mater*. 2016;407:308–313. https://doi.org/10.1016/j.jmmm.2016.01.099
7. Mishra RR, Sharma AK. Microwave–material interaction phenomena: Heating mechanisms, challenges and opportunities in material processing. *Compos Part Appl Sci Manuf*. 2016;81:78–97. https://doi.org/10.1016/j.compositesa.2015.10.035
8. Croquesel J, Bouvard D, Chaix J-M, Carry CP, Saunier S. Development of an instrumented and automated single mode cavity for ceramic microwave sintering:

Application to an alpha pure alumina powder. *Mater Des*. 2015;88:98–105. https://doi.org/10.1016/j.matdes.2015.08.122

9. Macaigne R, Marinel S, Goeuriot D, Meunier C, Saunier S, Riquet G. Microwave sintering of pure and TiO_2 doped $MgAl_2O_4$ ceramic using calibrated, contactless in-situ dilatometry. *Ceram Int*. 2016;42(15):16997–17003. https://doi.org/10.1016/j.ceramint.2016.07.206
10. van der Laag NJ, Snel MD, Magusin PCMM, de With G. Structural, elastic, thermophysical and dielectric properties of zinc aluminate ($ZnAl_2O_4$). *J Eur Ceram Soc*. 2004;24(8):2417–2424. https://doi.org/10.1016/j.jeurceramsoc.2003.06.001
11. Reimanis I, Kleebe H-J. A review on the sintering and microstructure development of transparent spinel ($MgAl_2O_4$). *J Am Ceram Soc*. 2009;92(7):1472–1480. https://doi.org/10.1111/j.1551-2916.2009.03108.x
12. Yong X, Ping F, Baohua Z, Juan G, Lin Z, Xuehua W. Optical properties of transparent $ZnAl_2O_4$ ceramics: A new transparent material prepared by spark plasma sintering. *Mater Lett*. 2014;123:142–144. https://doi.org/10.1016/j.matlet.2014.03.013
13. Ganesh I. A review on magnesium aluminate ($MgAl_2O_4$) spinel: synthesis, processing and applications. *Int Mater Rev*. 2013;58(2):63–112. https://doi.org/10.1179/1743280412Y.0000000001
14. Gajdowski C, Böhmler J, Lorgouilloux Y, Lemonnier S, d'Astorg S, Barraud E, Leriche A. Influence of post-HIP temperature on microstructural and optical properties of pure $MgAl_2O_4$ spinel: From opaque to transparent ceramics. *J Eur Ceram Soc*. 2017;37(16):5347–5351. https://doi.org/10.1016/j.jeurceramsoc.2017.07.031
15. Liu Y, Zhu J, Dai B. Transparent $MgAl_2O_4$ ceramics prepared by microwave sintering and hot isostatic pressing. *Ceram Int*. 2020;46(16):25738–25740. https://doi.org/10.1016/j.ceramint.2020.07.051

16. Talimian A, Pouchly V, El-Maghraby HF, Maca K, Galusek D. Transparent magnesium aluminate spinel: Effect of critical temperature in two-stage spark plasma sintering. *J Eur Ceram Soc*. 2020;40(6):2417–2425. https://doi.org/10.1016/j.jeurceramsoc.2020.02.012

17. Nečina V, Pabst W. Comparison of the effect of different alkali halides on the preparation of transparent $MgAl_2O_4$ spinel ceramics via spark plasma sintering (SPS). *J Eur Ceram Soc*. 2020;40(15):6043–6052. https://doi.org/10.1016/j.jeurceramsoc.2020.06.056

18. Obradović N, Fahrenholtz WG, Filipović S, Kosanović D, Dapčević A, Đorđević A, Balać I, Pavlović V.B. The effect of mechanical activation on synthesis and properties of $MgAl_2O_4$ ceramics. *Ceram Int*. 2019;45(9):12015–12021. https://doi.org/10.1016/j.ceramint.2019.03.095

19. Krell A, Waetzig K, Klimke J. Influence of the structure of $MgO{\cdot}nAl_2O_3$ spinel lattices on transparent ceramics processing and properties. *J Eur Ceram Soc*. 2012;32(11):2887–2898. https://doi.org/10.1016/j.jeurceramsoc.2012.02.054

20. Sokol M, Meir S, Strumza E, Kalabukhov S, Hayun S, Frage N. On the effects of LiF on the synthesis and reactive sintering of gahnite ($ZnAl_2O_4$). *Ceram Int*. 2017;43(17):14891–14896. https://doi.org/10.1016/j.ceramint.2017.08.005

21. Bykov YV, Egorov SV, Eremeev AG, Kholoptsev VV, Plotnikov IV, Rybakov KI, Sorokin AA, Balabanov SS, Belyaev AV. Ultra-rapid microwave sintering of pure and Y_2O_3-doped $MgAl_2O_4$. *J Am Ceram Soc*. 2018. https://doi.org/10.1111/jace.15788

22. Macaigne R, Marinel S, Goeuriot D, Saunier S. Sintering paths and mechanisms of pure $MgAl_2O_4$ conventionally and microwave sintered. *Ceram Int*. 2018;44(17):21107–21113. https://doi.org/10.1016/j.ceramint.2018.08.149

23. Kerbart G, Harnois C, Bilot C, Kerbart G. Pressure-assisted microwave sintering: A rapid process to sinter submicron sized grained $MgAl_2O_4$ transparent ceramics. *J Eur Ceram Soc*. 2019;39(9):2946–2951. https://doi.org/10.1016/j.jeurceramsoc.2019.03.046

24. Peillon N, Zuo F, Meunier C, Saunier S, Marinel S, Goeuriot D. In-situ studies on preparation of $ZnAl_2O_4$ spinel using microwave reactive sintering technique. *Mater Lett*. 2016;167:77–80. https://doi.org/10.1016/j.matlet.2015.12.143

25. Valdez Z, Aguilar J. Influence of Al_2O_3 on the production of $MgAl_2O_4$ with microwaves. 2000:72–74.

26. Li R, Liu J, Xu L, Zhou J. Microwave idrothermal synthesis of magnesium-aluminium spinel. *Ceram Int*. 2020;46(18):29207–29211. https://doi.org/10.1016/j.ceramint.2020.08.094

27. Aguilar JA, Gonzalez M, Gomez I. Microwaves as an energy source for producing magnesia-alumina spinel. *J Microw Power Electromagn Energy*. 1997;32(2):74–79. https://doi.org/10.1080/08327823.1997.11688326

28. Ganesh I, Srinivas B, Johnson R, Saha B. Microwave assisted solid state reaction synthesis of $MgAl_2O_4$ spinel powders. *J Eur Ceram Soc*. 2004;24(2):201–207. https://doi.org/10.1016/S0955-2219(03)00602-2

29 Peng Z, Hwang J-Y, Andriese M. Design of double-layer ceramic absorbers for microwave heating, *Ceram. Int.* 2013;39(6):6721–6725. http://dx.doi.org/10.1016/j.ceramint.2013.01.114.

30 Birnboim A, Gershon D, Calame J. Comparative study of microwave sintering of zinc oxide at 2.45, 30, and 83 GHz, *J. Am. Ceram. Soc.* 1998;81(6):1493-1501 https://doi.org/10.1111/j.1151-2916.1998.tb02508.x.

31. Żymełka D, Saunier S, Goeuriot D, Molimard J. Densification and thermal gradient evolution of alumina during microwave sintering at 2.45GHz. *Ceram Int*. 2013;39(3):3269–3277. https://doi.org/10.1016/j.ceramint.2012.10.015

32. Zuo F, Carry C, Saunier S, Marinel S, Goeuriot D. Comparison of the microwave and conventional sintering of alumina: Effect of MgO doping and particle size. *J Am Ceram Soc*. 2013;96(6):1732–1737. https://doi.org/10.1111/jace.12320

33. Jung I-H, Decterov SA, Pelton AD. Critical thermodynamic evaluation and optimization of the MgO-Al_2O_3, CaO-MgO-Al_2O_3, and MgO-Al_2O_3-SiO_2 Systems. *J Phase Equilibria Diffus*. 2004;25(4):329–345. https://doi.org/10.1007/s11669-004-0151-4

34. Hong W-S, De Jonghe LC, Yang X, Rahaman M.N. Reaction Sintering of ZnO-AI_2O_3. *J Am Ceram Soc*. 1995;78(12):3217–3224. https://doi.org/10.1111/j.1151-2916.1995.tb07957.x

35. Shiono T, Shiono K, Miyamoto K, Pezzotti G. Synthesis and characterization of $MgAl_2O_4$ spinel precursor from a heterogeneous alkoxide solution containing fine MgO powder. *J Am Ceram Soc*. 2000;83(1):235–37. https://doi.org/10.1111/j.1151-2916.2000.tb01180.x

36 Kassiba A, Tabellout M, Charpentier S, Herlin N, Emery JR. Conduction and dielectric behaviour of SiC nano-sized materials. *Solid State Commun.* 2000;115(7):389–393. https://doi.org/10.1016/S0038-1098(00)00195-2

Figures' and tables' captions

Table 1: Spinel content (%mol) in the ZnO/α-Al_2O_3 mixture heated up to 1150 °C under MW with and without SiC susceptor, with a heating rate of 50 °C/min.

Table 2: Spinel content (%mol) at 1400 °C after MW heating at different rates (°C/min) in three powder mixtures: (a) MgO/α-Al_2O_3, (b) MgO/γ-Al_2O_3 and (c) ZnO/α-Al_2O_3.

Table 3: Spinel content (%mol) in the three powders mixtures (MgO/α-Al_2O_3, MgO/γ-Al_2O_3, ZnO/α-Al_2O_3) heated up to 1400 °C at 25 °C/min in a CV or a MW furnace.

Figure 1: List of transitional alumina before reaching α-Al_2O_3 form by order of appearance with temperature rise.

Figure 2: Presentation of the MW device: (a) front view and (b) top view (adapted from Zuo *et al.*[32]).

Figure 3: XRD patterns of ZnO/α-Al_2O_3 samples heated with and without the SiC susceptor

Figure 4: Temperatures measured at the surface of ZnO/α-Al_2O_3 samples heated under MW with and without the SiC susceptor (with a heating rate set at 50 °C/min).

Figure 5: Instantaneous heating rate vs temperature for pellets heated with a constant MW incident power of 1200 W: (a) case of ZnO/α-Al_2O_3 with and without the SiC susceptor and (b) case of MW heating of ZnO/α-Al_2O_3 and MgO/γ-Al_2O_3 without the SiC susceptor.

Figure 6: XRD patterns of the samples after MW heating at different heating rates (10, 25 and 50 °C/min), (a) MgO/α-Al_2O_3, (b) MgO/γ-Al_2O_3 and (c) ZnO/α-Al_2O_3.

Figure 7: Spinel content (%mol) depending on temperature (°C) in three different powder mixtures: MgO/α-Al_2O_3, MgO/γ-Al_2O_3 and ZnO/α-Al_2O_3 under MW heating with a temperature ramp of 50 °C/min.

Figure 8: Spinel content (%mol) depending on time (a) and reaction rate constant k ($\%mol^{-1}.s^{-1}$) determined by linear regression (b) in three different powder mixtures: MgO/α-Al_2O_3, MgO/γ-Al_2O_3 and ZnO/α-Al_2O_3, heated with a MW source until 1350 °C, 1450 °C and 1150 °C respectively with a temperature ramp of 50 °C/min.

Figure 9: Linear regression of $1/[Al_2O_3] = f(t)$ to determine the reaction rate constant k ($\%mol^{-1}.s^{-1}$) of the transformation of MgO/α-Al_2O_3 into $MgAl_2O_4$ at 1350 °C and 1400 °C with a heating ramp of 50 °C/min.

Figure 10: Comparative study of MgO/γ-Al_2O_3 MW heating with a SiC susceptor and CV heating**,** with a temperature ramp of 25 °C/min: (a) without offset and (b) with an offset of -100 °C for MW heating data.

Table 4

Type of heating	Spinel content (%mol)
Hybrid	50.7
Direct	9.4

Table 5

Powder mixtures	**Phases**	**10 °C/min**	**25 °C/min**	**50 °C/min**
MgO/α-Al_2O_3	$MgAl_2O_4$	68.7	55.8	56.5
MgO/γ-Al_2O_3	$MgAl_2O_4$	59.7	46.0	40.0
ZnO/α-Al_2O_3	$ZnAl_2O_4$	92.9	95.3	91.9

Table 6

Heating process	**$MgAl_2O_4$ (α)**	**$MgAl_2O_4$ (γ)**	**$ZnAl_2O_4$**
CV	80.2	64.5	93.0
MW	55.8	46.0	95.3

Figure 1

Figure 2

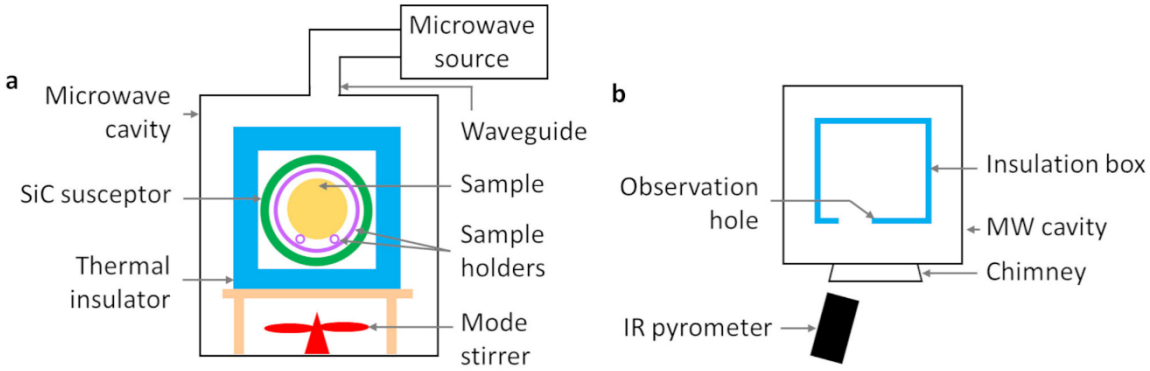
a
Microwave source
Microwave cavity
Waveguide
SiC susceptor
Sample
Sample holders
Thermal insulator
Mode stirrer
b
Observation hole
Insulation box
MW cavity
Chimney
IR pyrometer

Figure 3

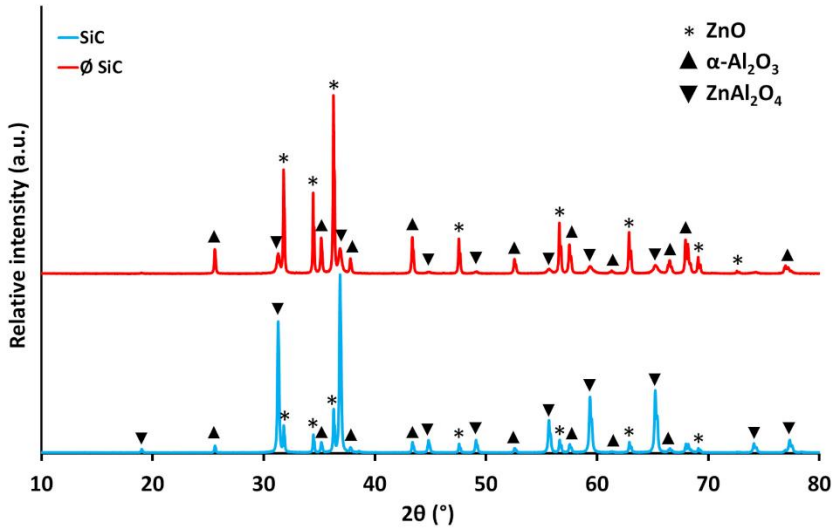
SiC
Ø SiC
* ZnO
▲ α-Al2O3
▼ ZnAl2O4
Relative intensity (a.u.)
10
20
30
40
50
60
70
80
2θ (°)

Figure 4

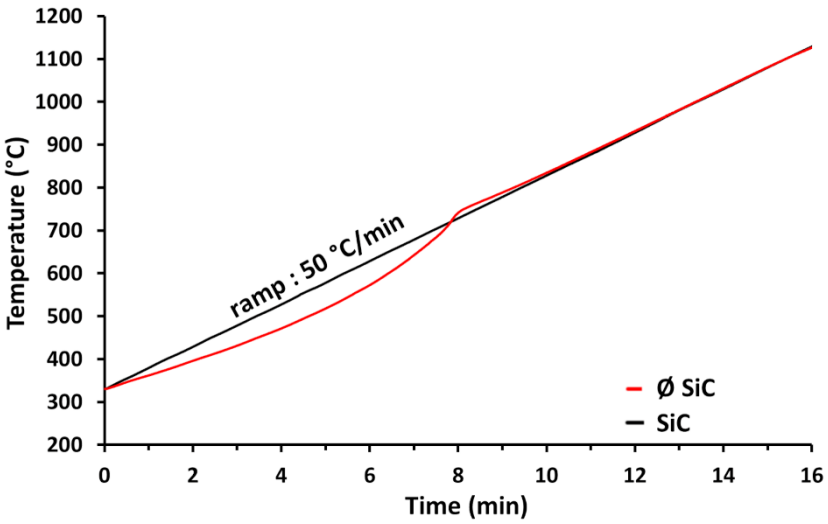
1200
1100
1000
900
800
700
600
500
400
300
200
Temperature (°C)
0
2
4
6
8
10
12
14
16
Time (min)
ramp : 50 °C/min
Ø SiC
SiC

Figure 5

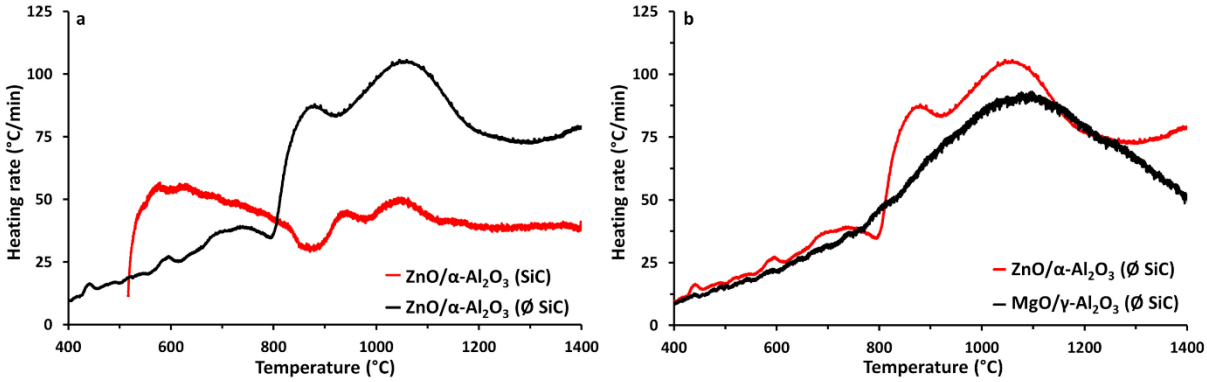
a
b
Heating rate (°C/min)
Temperature (°C)
ZnO/α-Al2O3 (SiC)
ZnO/α-Al2O3 (Ø SiC)
MgO/γ-Al2O3 (Ø SiC)

Figure 6

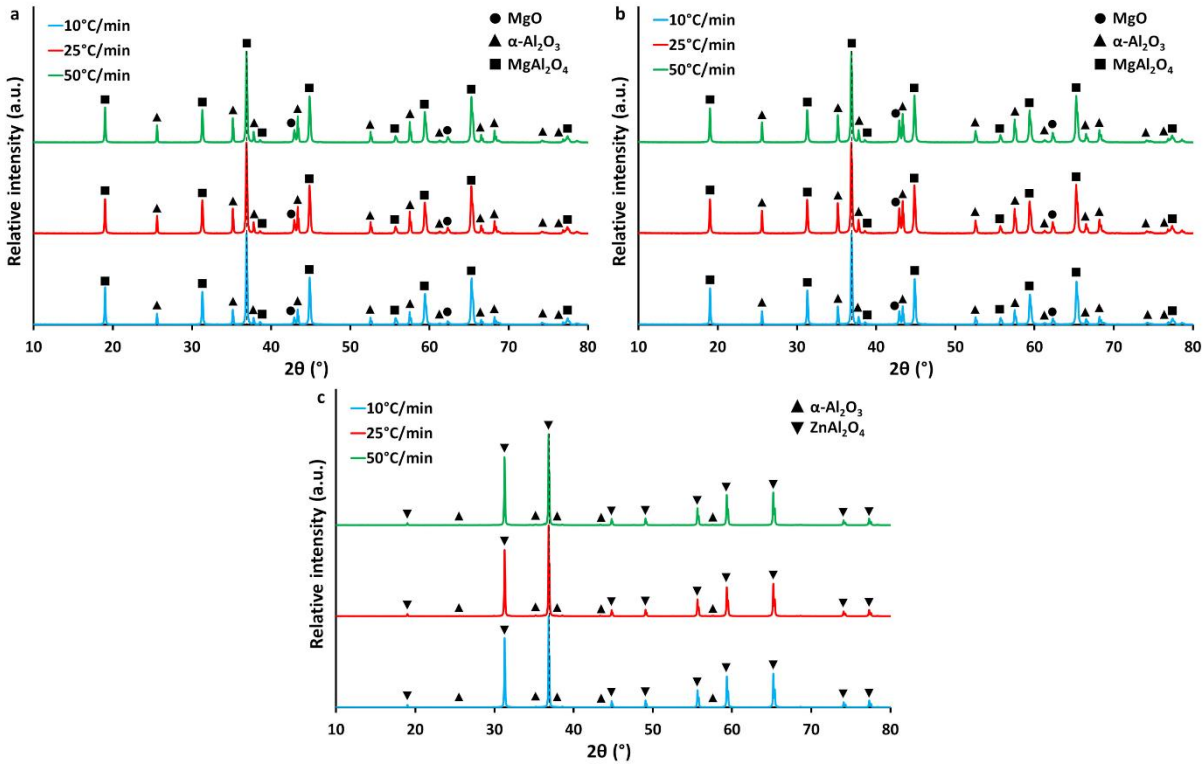
a
10°C/min
25°C/min
50°C/min
MgO
α-Al2O3
MgAl2O4
Relative intensity (a.u.)
2θ (°)
b
10°C/min
25°C/min
50°C/min
MgO
α-Al2O3
MgAl2O4
Relative intensity (a.u.)
2θ (°)
c
10°C/min
25°C/min
50°C/min
α-Al2O3
ZnAl2O4
Relative intensity (a.u.)
2θ (°)

Figure 7

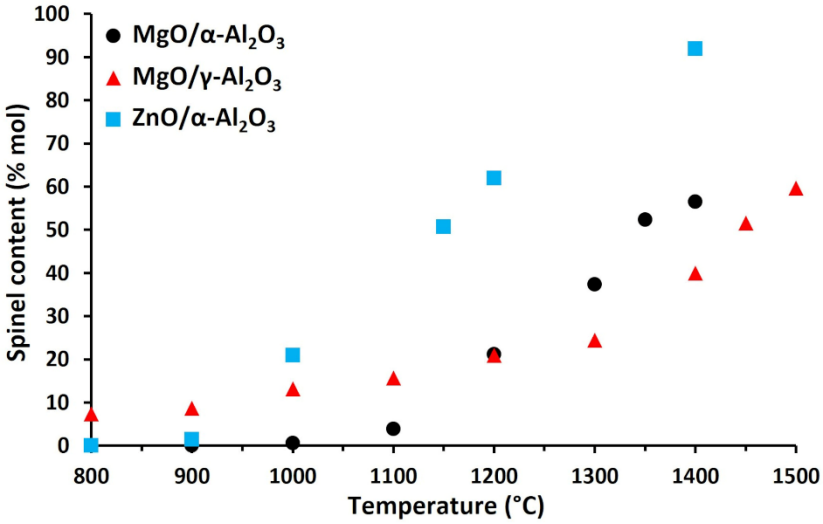
MgO/α-Al2O3
MgO/γ-Al2O3
ZnO/α-Al2O3
Spinel content (% mol)
Temperature (°C)
0
10
20
30
40
50
60
70
80
90
100
800
900
1000
1100
1200
1300
1400
1500

Figure 8

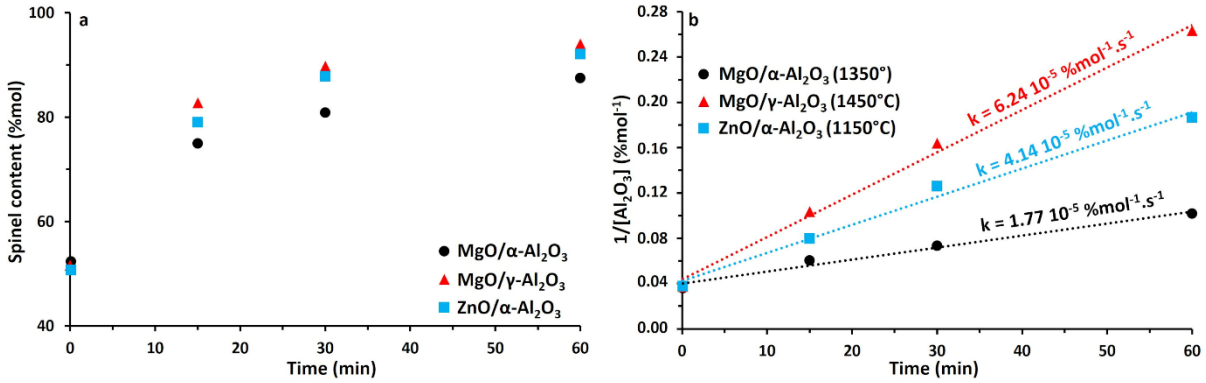
a
Spinel content (%mol)
Time (min)
MgO/α-Al2O3
MgO/γ-Al2O3
ZnO/α-Al2O3
b
1/[Al2O3] (%mol-1)
Time (min)
MgO/α-Al2O3 (1350°)
MgO/γ-Al2O3 (1450°C)
ZnO/α-Al2O3 (1150°C)
k = 6.24 10-5 %mol-1.s-1
k = 4.14 10-5 %mol-1.s-1
k = 1.77 10-5 %mol-1.s-1

Figure 9

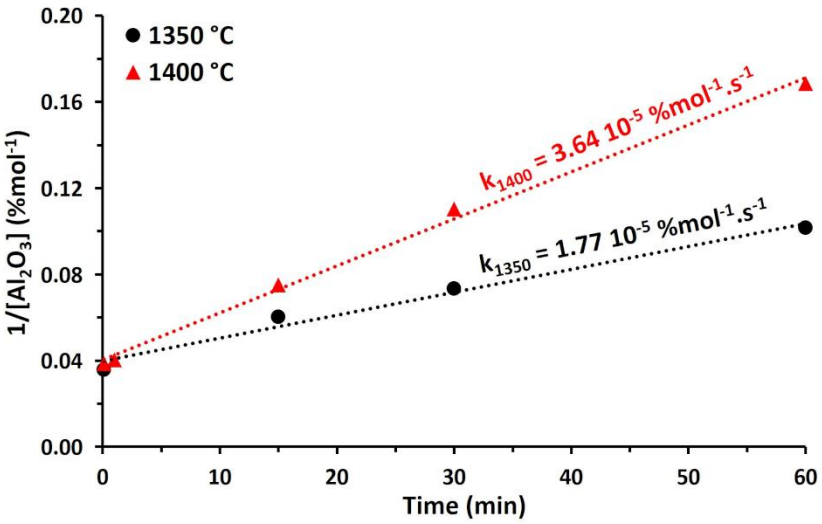
0.20
0.16
0.12
0.08
0.04
0.00
1/[Al2O3] (%mol-1)
1350 °C
1400 °C
k1400 = 3.64 10-5 %mol-1.s-1
k1350 = 1.77 10-5 %mol-1.s-1
0
10
20
30
40
50
60
Time (min)

Figure 10

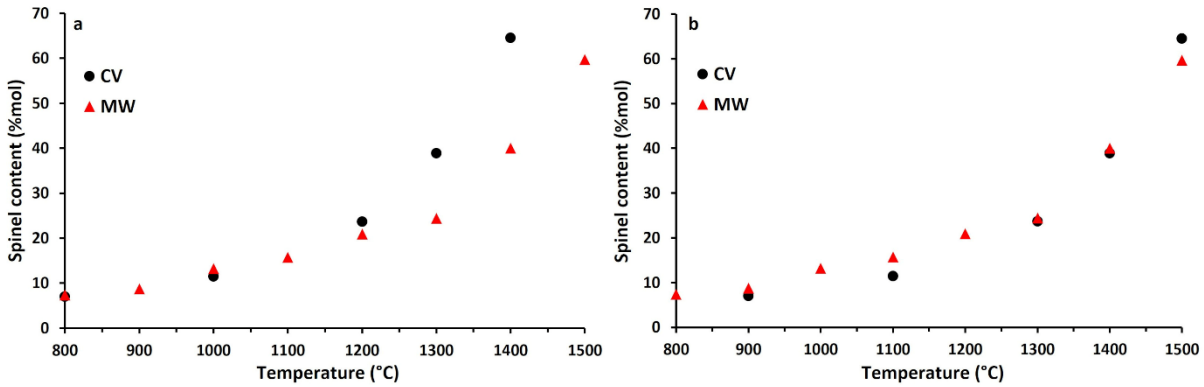
a
CV
MW
Spinel content (%mol)
Temperature (°C)
b
CV
MW
Spinel content (%mol)
Temperature (°C)